Effect of activation energy on detonation re-initiation behaviors in hydrogen-air mixtures

Shizhi Tang, Shiyan Zhang, and Shuyue Lai*
School of Aeronautics and Astronautics, Shanghai Jiao Tong University (SJTU), Shanghai, People's Republic of China

Chao Xu
Transportation and Power Systems Division, Argonne National Laboratory, Lemont, IL 60439, USA

Xiaohang Fang
Department of Mechanical & Manufacturing Engineering, Schulich School of Engineering, University of Calgary, T2L 1Y6, Calgary, Canada

Two-dimensional simulations of a detonation propagating over a semi-cylinder in a channel filled with a stoichiometric hydrogen-air mixture are presented. A full set of Navier-Stokes equations is solved using a third-order WENO algorithm with HLLC flux, coupled with a calibrated, single-step chemical diffusive model (CDM). Simulation results using five different effective activation energies $\mathcal{E}$ = 4, 6, 10, 12 and 14 are presented featuring four distinct detonation attenuation regimes, including unattenuated detonation transmission ($\mathcal{E}$ = 4), critical detonation re-initiation ($\mathcal{E}$ = 6, and 10), cycled detonation re-initiation ($\mathcal{E}$ = 12), and complete quenching ($\mathcal{E}$ = 14). The degree of cell irregularity and the intensity of triple points are found positively correlated with the effective activation energy. With a low effective activation energy ($\mathcal{E}$ = 4), the CDM captures a regular cellular pattern, and the cellular structure remains intact as it propagates over the obstacle. With intermediate effective activation energies ($\mathcal{E}$ = 6, and 10), the detonation cell size increases and the cell structures become less regular with emerging multi-level cell structures. Here, a critical detonation re-initiation event is captured, where a strong transverse detonation wave forms following the Mach shock reflection, and eventually leads to a steady detonation propagation. At high effective activation energy ($\mathcal{E}$ = 12), the initial transverse detonations fail to produce a self-sustained detonation wave and multiple ignition and quenching events are found before the final establishment of the detonation wave.

I. Introduction

Understanding detonation waves interacting with obstacles is critical for the study of detonation wave propagation. Under proper conditions, when a detonation wave diffracts from an obstacle, it may first quench and then re-initiate. This phenomenon is first captured by a series of Schlieren photographs in an early experiment performed by Teodorczyk et al. [1], and has been investigated both experimentally and numerically using different types of obstacles, such as a single semi-cylindrical obstacle [2–4], a series of small cylindrical obstacles [5], and a porous plate [6, 7]. Upon these investigations, researchers have found several mechanisms that may contribute to the re-initiation. Ohyagi et al. [8] found that there is a trace of a transverse wave upstream of the re-constructed detonation wave in the soots-track records, indicating that this transverse wave might serve as a trigger for the re-initiation. Further studies [5–7] suggested that the transverse pressure waves behind the Mach shock can lead to pressure amplification, which might be a possible reason for re-initiation. Meanwhile, there was another opinion that regarded the turbulent mixing caused by the wall jet or the Kelvin-Helmholtz instability behind the Mach shock as a major reason for the re-initiation [2, 3]. If the turbulent mixing behind the Mach shock is intense enough, it can dramatically promote the chemical reaction by rapidly mixing the cold unburned gas and the hot burned gas, and thus induces a detonation re-initiation. Recently, Floring et al. [4] comprehensively revisited the behaviors when an established cellular detonation wave passes through a semi-cylindrical obstacle, highlighting the role of a transverse detonation wave in re-initiation events. Taking a detailed analysis of critical outcomes captured by varying the initial background pressure, they suggested that the pressure amplification behind the Mach shock might induce hot spots around the flame surface. These hot spots can develop into a transverse detonation by the Zeldovich gradient mechanism and consequently trigger the re-initiation.

*Corresponding Author; laishuyue@sjtu.edu.cn

For numerical studies investigating the re-initiation events, different chemical reaction models have been adopted, among which the one-step chemical model that follows the Arrhenius form has been used extensively [3, 5]. However, the one-step model failed to capture the main properties of combustion such as the induction time, as well as the detonation initiation process. For example, using such model, Radulescu and Maxwell [5] only generated an inert transverse wave instead of a transverse detonation wave, which is considered to be crucial in detonation re-initiation. A single-step chemical diffusive model (CDM), developed by Oran and Gamezo [9] has been widely used to investigate the DDT process and is able to correctly capture the key features of combustion in both flame and detonation regimes [10]. Recently, the input parameters for the CDM has been calibrated and optimized with emphasis on detonation wave properties [11], and the model has shown great potential in capturing the detonation propagation and quenching event. The most important factor that governs the one-step model is the effective activation energy ($\mathcal{E}$) and many previous studies [11–14] emphasized on the effect of $\mathcal{E}$ on the dynamics of a detonation wave. In general, with a high effective activation energy, the chemical reaction time is sensitive to temperature, and thus, the appearance, merging, bifurcation, and disappearance of triple points occur more frequently and finally lead to the irregularity in detonation cellular structure. However, there is still a lack of systematic studies on the effect of effective activation energy on the detonation decoupling and re-initiation process.

The purpose of this paper is to numerically evaluate the effect of different effective activation energies on the detonation cellular dynamics for the hydrogen-air detonation attenuation problem. Specifically, we investigate how the cell size and structures change with an increasing $\mathcal{E}$ for the one-step chemical diffusive model. In addition, the behavior of detonation decoupling and re-initiation when a cellular detonation wave diffracts from a cylindrical obstacle is studied with emphasis on the role of effective activation energy on the critical outcomes of detonation re-initiation. The structure of the paper is as follows: The governing equations and the chemical model are first described in detail in Section II. The effect of effective activation energy on detonation cellular structure is discussed in Section III A. Then critical detonation re-initiation outcomes using different effective activation energies are analyzed in Section III B. Finally, detonation re-initiation mechanisms are further detailed in Section III C.

II. Numerical and Physical Models

A. Governing equations and chemical-diffusive model

In this paper, we solve the Navier-Stokes equations for a two-dimensional, fully compressible, reactive flow, which include the conservation laws for mass, momentum, energy, and species [15, 16]:

$$\frac{\partial \rho}{\partial t} + \nabla \cdot (\rho \mathbf{U}) = 0 \tag{1}$$

$$\frac{\partial (\rho \mathbf{U})}{\partial t} + \nabla \cdot (\rho \mathbf{U}\mathbf{U}) + \nabla p + \nabla \cdot \hat{\boldsymbol{\tau}} = 0 \tag{2}$$

$$\frac{\partial (\rho E)}{\partial t} + \nabla \cdot ((\rho E + p)\mathbf{U}) + \nabla \cdot (\mathbf{U} \cdot \hat{\boldsymbol{\tau}}) + \nabla \cdot (K \nabla T) + \rho q \dot{\omega} = 0 \tag{3}$$

$$\frac{\partial (\rho Y)}{\partial t} + \nabla \cdot (\rho Y \mathbf{U}) + \nabla \cdot (\rho D \nabla Y) - \rho \dot{\omega} = 0 \tag{4}$$

where ρ, $\mathbf{U}$, p, T, and Y represent the density, velocity, pressure, temperature, and mass fraction of the reactant, respectively. $\dot{\omega}$ is the chemical reaction rate, E is the fluid energy density, q is the chemical energy release, K is the thermal conductivity, and D is the mass diffusivity.

The gas equation of state follows the ideal gas law,

$$p = \frac{\rho R T}{M} \tag{5}$$

where R is the specific gas constant, and M is the molecular weight.

The specific energy density E is calculated from

$$E = \frac{p}{(\gamma - 1)\rho} + \frac{1}{2}(\mathbf{U} \cdot \mathbf{U}) \tag{6}$$

where γ is the specific heat ratio.

Table 1 CDM input parameters [11]

Symbol	Description	Value	Unit
p_0	Initial pressure	1	atm
T_0	Initial temperature	298	K
M_w	Molecular weight	27	g/mol
γ	Specific heat ratio	1.33	
q	Relative heat release	26.33	RT_0/M_w
κ_0	Reference thermal diffusivity	2.54×10^{-6}	g/s cm $K^{0.7}$

Table 2 Reaction properties with different effective activation energy [11]

$\mathcal{E} = E_a/(RT_{vn})$	4	6	10	12	14	
E_a	25.7	38.5	63.8	76.1	91.0	(RT_0)
A	1×10^6	4.55×10^6	1.5×10^8	8.5×10^8	6.8×10^9	(m^3/g s)

The viscous stress tensor is defined as

$$\hat{\tau} = \rho\nu((\nabla\mathbf{U}) - (\nabla\mathbf{U})^T - \frac{2}{3}(\nabla\cdot\mathbf{U})\mathbf{I}) \tag{7}$$

where ν is the kinematic viscosity, $\mathbf{I}$ is the unit tensor, and the superscript T denotes the matrix transpose.

To simulate the premixed stoichiometric combustion of hydrogen-air mixture, we adopt a calibrated, one-step chemical-diffusive model (CDM) [17] where the reaction rate is governed by a first-order Arrhenius equation:

$$\dot{\omega} = -A\rho Y\exp(-E_a/RT) \tag{8}$$

where A is a pre-exponential factor and E_a represents the activation energy. The viscosity, mass diffusivity, and thermal diffusivity in CDM are sensitive to temperature in a similar form:

$$\nu = \nu_0\frac{T^n}{\rho}, \quad D = D_0\frac{T^n}{\rho}, \quad \frac{K}{\rho C_p} = \kappa_0\frac{T^n}{\rho} \tag{9}$$

where ν_0, D_0, κ_0 are transport constants, $C_p = \gamma R/M(\gamma-1)$ represents the specific heat at constant pressure. In reactive hydrocarbon systems, n is typically chosen as 0.7. The non-dimensional numbers characterizing the system, including Lewis, Prandtl, and Schmidt numbers, are independent of thermodynamic conditions:

$$Le = \frac{K}{\rho C_p D} = \frac{\kappa_0}{D_0}, \quad Pr = \frac{\rho C_p \nu}{K} = \frac{\nu_0}{\kappa_0}, \quad Sc = \frac{\nu}{D} = \frac{\nu_0}{D_0} \tag{10}$$

For simplicity, in this study, all of these non-dimensional numbers are unity.

The effective activation energy is defined as

$$\mathcal{E} = \left.\frac{d\ln\tau}{d1/T}\right|_{T_{vn}} = \frac{E_a}{RT_{vn}}, \tag{11}$$

where T_{vn} is the post-shock temperature in a ZND structure, and τ is the induction time.

The input parameters for the CDM shown in Table 1 and 2 are determined by Lu et al. [11], and are calibrated to reproduce the flame and detonation properties of the hydrogen-air mixture initially at 1 atm and 298 K. Specifically, five different effective activation energies $\mathcal{E}$ = 4, 6, 10, 12, and 14 are considered in this study. Several previous studies have demonstrated that the one-step chemical model, along with the chosen parameters, effectively captures the key features of various problems, including laminar flame propagation, shock-flame interactions, and detonations [16, 18, 19].

The governing equations are solved using a third-order WENO algorithm with HLLC fluxes for spatial discretization and a third-order Runge-Kutta scheme for time advancement. The grid size for the numerical simulations is dx = 200 μm, which is adequate to capture the important flame properties for detonation propagation, decoupling, and re-initiation.

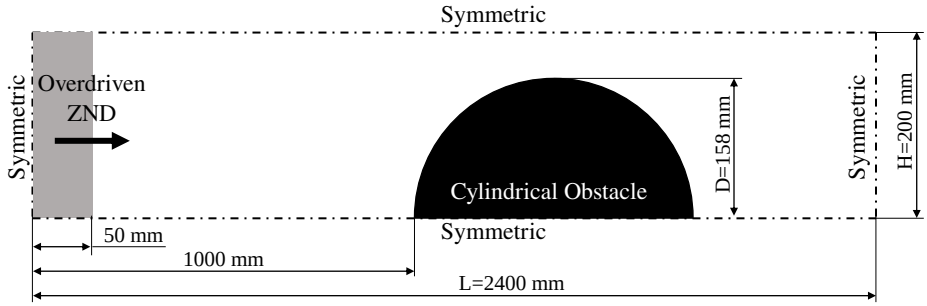

Fig. 1 A schematic of computational domain and initial conditions of numerical simulations.

B. Physical models

The computational domain is shown in Fig. 1, where the geometries correspond to previous experiments [2, 3]. The simulation involves a channel of 2.4 m in length and 20 cm in height. To initiate a cellular detonation wave, an overdriven Zel'dovich-von Neumann-Döring (ZND) structure with an overdriven factor $f = 1.3$ is placed at the left boundary of the domain. Both the top and bottom boundaries are symmetric and the surface of the obstacle is a no-slip, adiabatic wall. The initial background temperature and pressure are 298 K and 1 atm, respectively. A semi-cylindrical obstacle is placed at $x = 1.0$ m and the radius of the obstacle is 15.8 cm, corresponding to a blockage ratio of 0.79. The leading edge of the cylinder was positioned 1 m away from the initial overdriven ZND wave. This distance was determined to be sufficiently long to allow the detonation wave to stabilize to CJ-detonation speed by the time it reached the throat of the cylinder, regardless the effective activation energies were chosen.

III. Results and Discussions

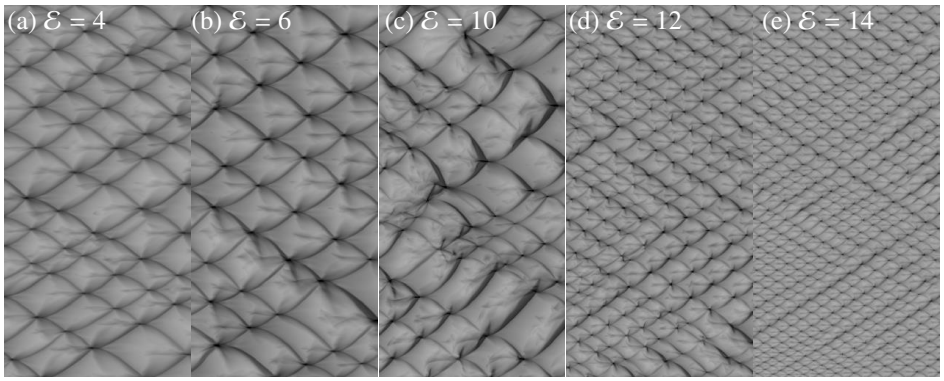

Fig. 2 Numerical soot foils showing the cellular structures of the detonation waves for cases of (a) $\mathcal{E} = 4$, (b) $\mathcal{E} = 6$, (c) $\mathcal{E} = 10$, (d) $\mathcal{E} = 12$, and (e) $\mathcal{E} = 14$. Dimension of each frame are 10 × 20 cm.

A. Detonation cell structures

Fig. 2 shows the numerical smoke foils using all five different activation energies at the location from $x = 0.8$ m to $x = 0.9$ m. For $\mathcal{E} = 4, 6, 10$, as the effective activation energy increases, the cellular structure becomes more irregular, and detonation cell size slightly increases. In addition, the detonation cell begins to develop multi-level structures. For $\mathcal{E} = 12$ and $\mathcal{E} = 14$, however, the detonation cell structures are significantly smaller than the rest of the results. This aligns with earlier numerical simulations, wherein an increase in the activation energy of the model results in a bifurcation of cell sizes, accompanied by a growing unpredictability in the dynamics [20]. One of the reasons could be simulations with a higher activation energy will require a much finer grid to resolve the smaller induction length and the current resolution is insufficient to resolve the detonation structures for these two cases as suggested by earlier study [11].

The need for increased resolution with higher activation energy is caused by the exponential expansion of the range of reaction zone length scales, which corresponds to various shock temperatures attained in the cellular detonation, directly proportional to the activation energy. Nevertheless, the degree of cell irregularity and the intensity of triple points found in this study positively correlated with the effective activation energy which is consistent to previous studies [12].

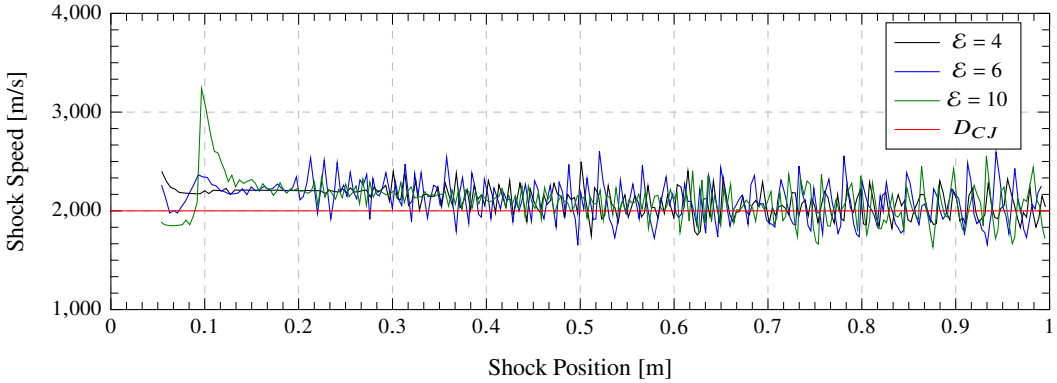

Fig. 3 Speed of the leading shock for cases of $\mathcal{E} = 4$, $\mathcal{E} = 6$, and $\mathcal{E} = 10$ in comparison with the CJ detonation speed.

The speed of the detonation waves for the case of $\mathcal{E} = 4, 6, 10$ is shown in Fig. 3 with a comparison to the CJ detonation speed. Initially, the detonation propagates with a high velocity and then gradually settles to D_{CJ}. It is found that with a higher $\mathcal{E}$, a longer time is needed for the detonation wave to reach a steady mode. With an increased effective activation energy, the detonation cell grows faster at the initial stage. However, the increasing irregularity of the cell structure together with the emerging second-level structures with higher $\mathcal{E}$ results in a longer settling time. Nevertheless, an overdrive factor of 1.3 is found sufficient to overcome the startup errors associated with sharp discontinuities where for all effective activation energies the detonation waves are stabilized to CJ-detonation speed by the time they reach the throat of the cylinder at 1 m.

B. Critical outcomes

Early studies have suggested that the stability of the detonation is sensitive to the activation energy [20, 21]. In this section, we present an overview of various outcomes observed in detonation waves resulting from variations in effective activation energy. Fig. 4 shows the numerical soot foil images for cases of $\mathcal{E} = 4, 6, 10, 12, 14$. These images were generated by capturing the maximum locally experienced pressure at each grid point during the simulation. As the highest pressures occur at triple point locations, where the incident, Mach, and transverse shocks converge, this approach effectively monitors the paths of triple points. For all listed cases, as the detonation front expands beyond the obstacle, a larger shock surface area forms. This expanded area causes a reduction in shock strength, leading to prolonged ignition delay times and, consequently, an increased distance between the shock front and the reaction zone leading to various regimes for different effective activation energies.

For a low effective activation energy, $\mathcal{E} = 4$, the detonation wave exhibits unattenuated detonation transmission, with no notable instances of quenching observed in the soot foil image. The cellular structure remains intact across both the length and height of the channel. This is consistent with previous one-dimensional detonation studies suggesting that as the activation energy decreases, the steady wave structure and the primary heat release layer become longer. Concurrently, the peak of the maximum reaction rate decreases due to the weakened exponential sensitivity of the reaction rate to local thermodynamic variations [21]. When effective activation energy increases and falls into a specific range, specifically, for $\mathcal{E} = 6$ and $\mathcal{E} = 10$, critical detonation re-initiation is found where the attenuated detonation is found to be reinitiated featuring one or more transverse detonations. For both cases, there is a triangular area without any triple points formed immediately after the obstacle, indicating partial quenching. The partial quenching area is followed by transverse detonations characterized by dark bands that started near the lower boundary and propagated upwards. Specifically, it is observed that a shock reflection at bottom boundaries drives local pressure waves outward, facilitating their coupling with the rapid energy release resulting from chemical reactions. This reflection generated a transverse detonation wave moving upwards, followed by the formation of a cellular structure. The critical detonation reinitiation event is therefore characterized by a spatial region of quenching, succeeded by reinitiation featuring a pronounced

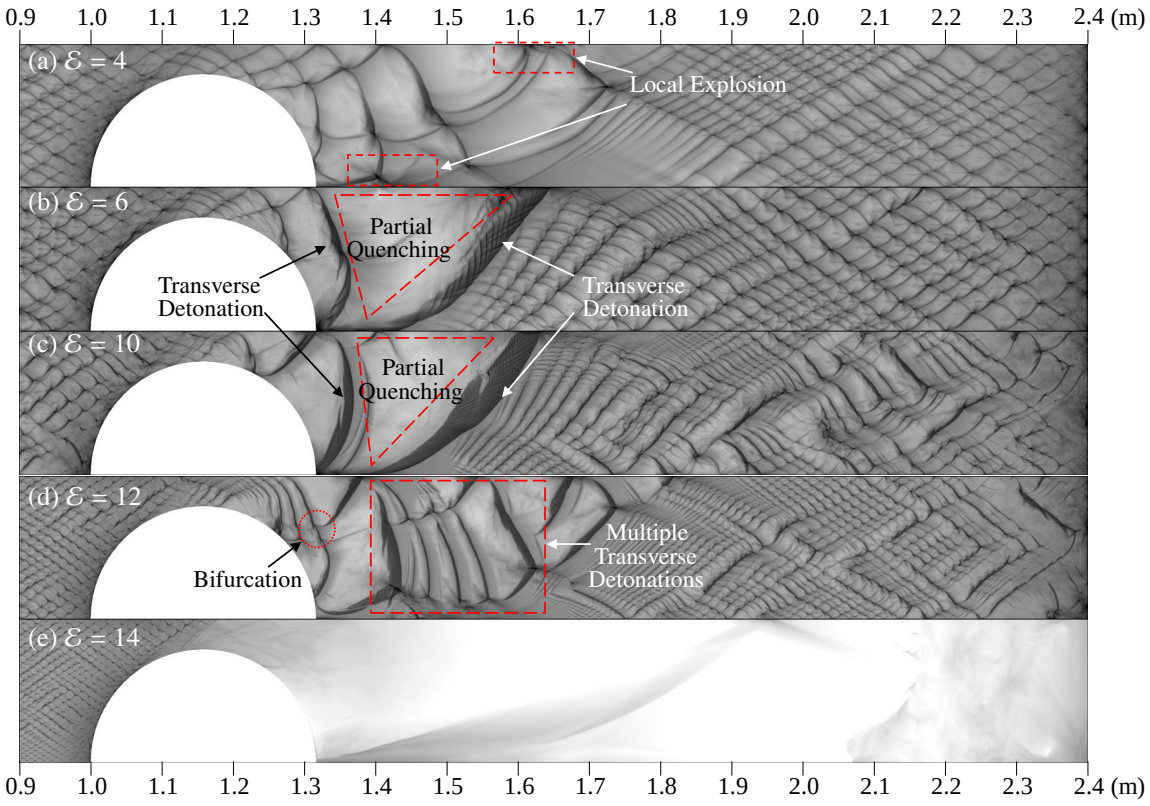

Fig. 4 Numerical soots-track records showing different detonation behavior regimes for cases of (a) $\mathcal{E}$ = 4, (b) $\mathcal{E}$ = 6, (c) $\mathcal{E}$ = 10, (d) $\mathcal{E}$ = 12 and (e) $\mathcal{E}$ = 14. Dimension of smoke foils are 1.5 m $\times$ 20 cm.

transverse detonation.

When the effective activation energy is high enough, the process of detonation re-initiation changes. For $\mathcal{E}$ = 12, when the detonation wave diffracts from the obstacle, there are still several triple points remaining. Different from cases of $\mathcal{E}$ = 6 and $\mathcal{E}$ = 10 mentioned above, there is a bifurcation of a triple point, which turned this triple point into two. Both of the triple points reflected from the obstacle surface and the upper boundary, respectively, forming transverse detonations, which then reflected from the boundaries several times, as a consequence, one of these transverse detonation waves generates a cellular detonation wave and triggers the re-initiation. This also corresponds well with previous one-dimensional detonation studies suggesting with increasing effective activation energies smaller amounts of exothermicity are required to generate instability [21]. For an even higher effective activation energy, $\mathcal{E}$ = 14, the detonation undergoes complete quenching immediately after surpassing the obstacle. Detonation quenching occurs when the cellular pattern vanishes, indicating a separation of the shock front and reaction zone that is never re-established into a detonation. According to prior experimental investigations focused on visualizing the diffracted detonation waves and reaction zone structures, it is observed that the velocity of the reaction front on the centerline decays notably more rapidly in mixtures characterized by higher activation energy [22].

C. Detonation re-initiation

In order to further detail the process of detonation re-initiation temperature and numerical Schlierens fields of three effective activation energies are depicted. Fig. 5 shows the time series of temperature fields for cases of $\mathcal{E}$ = 6 and $\mathcal{E}$ = 10. As discussed above, the process of detonation re-initiation for $\mathcal{E}$ = 6 and $\mathcal{E}$ = 10 is similar to each other. For both of cases, after the detonation wave passed through the obstacle, it decoupled into a transverse detonation moving downward, as shown in the first column in Fig. 5. And then it reflected from the bottom boundary, generating a new transverse detonation wave moving upward. When this transverse detonation wave moved upward, new triple points appeared ahead of this transverse detonation wave, as shown in the last two columns in Fig. 5. As the transverse

detonation wave reached the upper boundary, a cellular detonation wave that filled the height of the channel was formed. The results in these two effective activation energies correspond well with previous numerical research where transverse detonation is found to play a positive role in assisting detonation reinitiation in a variety of different configurations [4].

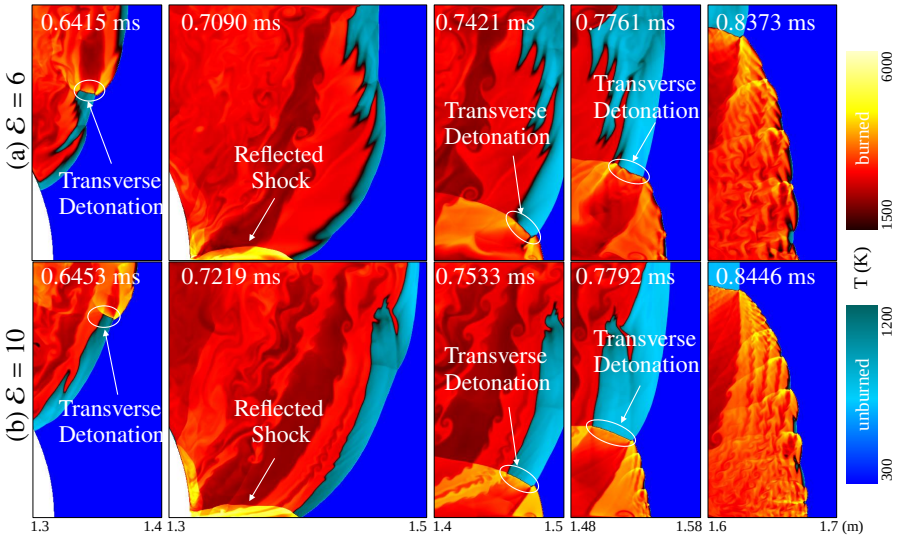

Fig. 5 Temperature fields at different times showing the process of critical detonation re-initiation for cases of (a) $\mathcal{E}$ = 6 and (b) $\mathcal{E}$ = 10.

The time history of temperature fields and numerical Schlieren images for the case of $\mathcal{E}$ = 12 are shown in Fig. 6 and Fig. 7. After the expansion from the obstacle, at about 0.6235 ms, most of the transverse detonation waves decoupled except the front-most one. A local explosion, which is exactly the "Bifucation" marked in Fig. 4 (d), turned this transverse detonation into two moving in the opposite direction. At 0.6425 ms transverse detonations started at the center and propagated toward the upper and lower boundaries of the channel which defers from lower effective activation energies where transverse detonations started near the lower boundary and propagated upwards. At about 0.6678 ms, one of the transverse detonations reflected from the surface of the obstacle while the other reflected from the upper boundary. More transverse detonation waves were generated due to the reflections, bifurcations, and collisions of transverse detonations. At 0.7958 ms shown in numerical Schlieren image, two triple points have formed due to the propagation of reflected waves from both the top and bottom boundaries of the simulation forming new transverse detonation waves. These triple points traveled toward each other and eventually collided. This caused the formation of new reflected waves with increased temperature and pressure behind them. Finally, detonation reinitiations along both the Mach and transverse waves are indicated by cellular patterns as shown in both temperature and numerical Schlieren images at 0.8582 ms. The two-dimensional detonation wave characteristics clearly demonstrated that cell irregularity and the intensity of triple points are more profound in higher effective activation energy. Such behavior corresponds well with previous one-dimensional nonlinear dynamics studies on the one-step Arrhenius chemistry detonation model [23]. It was suggested that with an increase in activation energy, the one-dimensional detonation front may transition from a stable solution to an oscillatory pattern characterized by limit cycle oscillation. As the activation energy continues to rise, subsequent period doublings occur rapidly, leading these one-dimensional oscillations to follow the classical Feigenbaum route to chaos.

Fig. 8 shows the speed of the leading shock wave vs. x position along the channle obtained along the bottom boundary at y= 0, for cases of $\mathcal{E}$ = 4, $\mathcal{E}$ = 6, $\mathcal{E}$ = 10, $\mathcal{E}$ = 12 and $\mathcal{E}$ = 14. Clear differences are observed between each case. For $\mathcal{E}$ = 4, while previous soot foil suggested the detonation wave exhibits unattenuated detonation transmission, it was found through the shock speed that decoupling between the reaction zone and the shock front also happened immediately after the obstacle indicated by the drop in shock speed below CJ speed. While no transverse detonation is found, the reinitiation can be associated with localized explosions that occurred near the top and bottom boundaries as highlighted in Fig. 4 (a). For $\mathcal{E}$ = 6, at around x = 1.3 m, there is a dramatic drop in shock speed, which is suggested by the partial quenching shown in Fig. 4 (b). Soon after this drop, at around x = 1.6 m, the shock speed increased sharply owing to the reinitiation event given by the transverse detonation and then kept oscillating around the CJ speed.

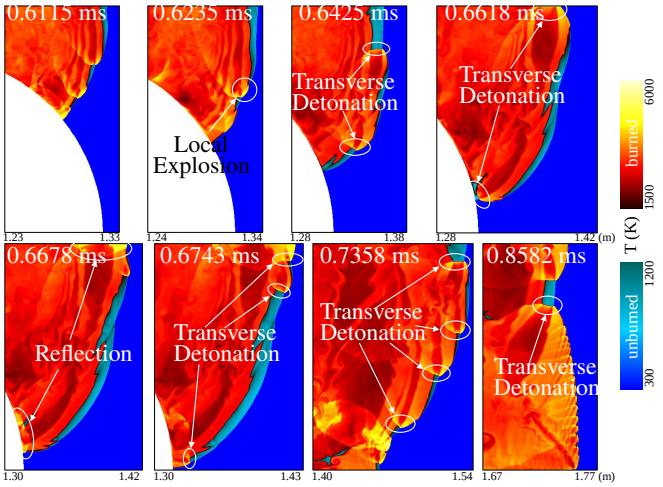

Fig. 6 Temperature fields at different times showing the process of detonation re-initiation for the case of $\mathcal{E} = 12$.

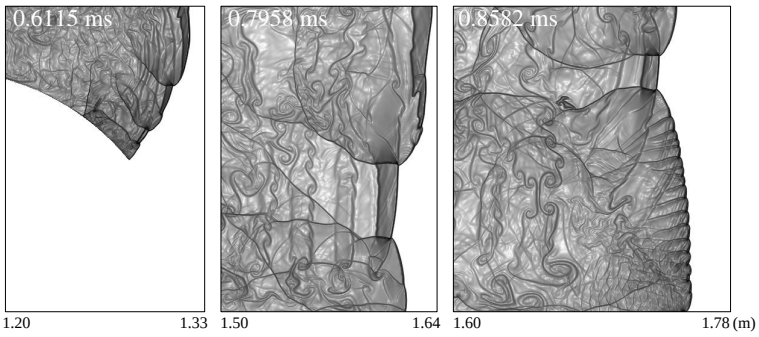

Fig. 7 Numerical schlieren fields at different times showing the process of detonation re-initiation for the case of $\mathcal{E} = 12$.

For $\mathcal{E} = 10$ and $\mathcal{E} = 12$, at the first re-initiation event (at $x = 1.4$ m), there was a sudden dramatic increase in shock speed. However, the detonation was not sustained as suggested by the shock speed. Multiple increases and drops are evident until around 1.6 m caused by multiple reinitiation events where near 1.7 m detonation is stabilized. Beyond this distance, the detonation eventually settled and oscillated around the CJ speed once again. For $\mathcal{E} = 14$, the detonation wave immediately quenched at about $x = 1.2$ m and the shock speed decreased dramatically after its interaction with the obstacle. The speed of the leading shock wave along the bottom boundary after shock reflection never reached the theoretical CJ speed. It is clear from the shock speed results that as the effective activation energy increases, growing unpredictability in the dynamics is seen in the detonation structure which results in multiple shock flame decoupling and reinitiations.

IV. Summaries and Conclusions

This paper numerically investigates the detonation attenuation and re-initiation process of hydrogen-air mixtures over a cylinder by solving a full set of Navier-stokes equations using a third order WENO algorith. A newly calibrated, one-step chemical diffusive model is used with a variation of effective activation energies $\mathcal{E} = 4$, 6, 10, 12 and 14. First, the detonation cell structures using different effective activation energies are examined. The results show that with an increase of effective activation energy for $\mathcal{E} = 4$, 6, and 10, the cellular structure experiences a growth of inregularity and multi-level structures are observed. For the case of $\mathcal{E} = 12$, and 14, the detonation cell structures are significantly smaller with bifurcation of cell sizes, accompanied by a growing unpredictability in the detonation cellular dynamic. The results demonstrated in this study suggest the degree of cell irregularity and the intensity of triple points

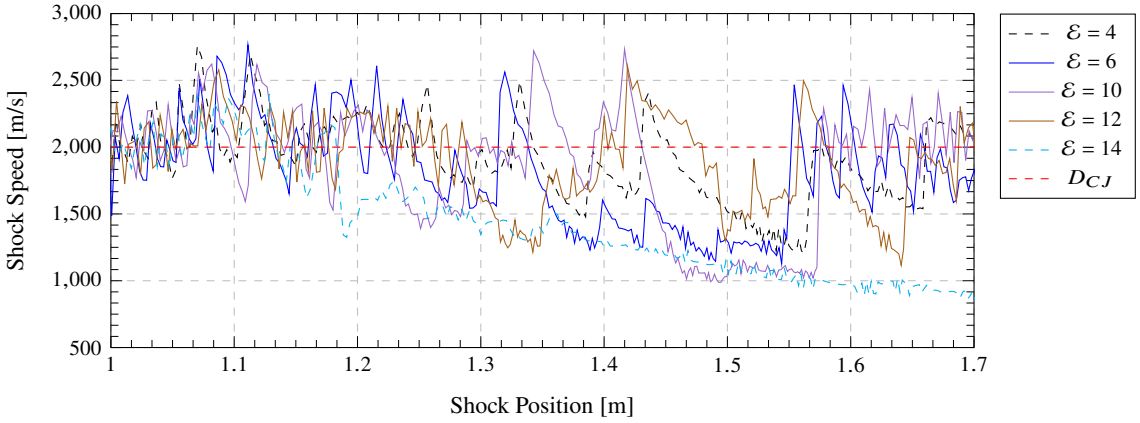

Fig. 8 Speed of the leading shock for cases of $\mathcal{E} = 4$, $\mathcal{E} = 6$, $\mathcal{E} = 10$, $\mathcal{E} = 12$, and $\mathcal{E} = 14$ in comparison of the CJ detonation speed.

are positively correlated with the effective activation energy. With the examined detonation wave structures after its attenuation by the cylinder, several critical outcomes including unattenuated detonation transmission ($\mathcal{E} = 4$), critical detonation re-initiation ($\mathcal{E} = 6$, and 10), cycled detonation re-initiation ($\mathcal{E} = 12$), and complete quenching ($\mathcal{E} = 14$) are captured for the detonation attenuation problem. In addition, the detonation re-initiation mechanism is further detailed. For the critical re-initiation event ($\mathcal{E} = 6$, and 10), a strong transverse detonation wave is observed following the Mach shock reflection, moving upwards, and leading to the re-establishment of a self-sustained detonation wave. As a contrast, for the case of $\mathcal{E} = 12$, multiple transverse detonation waves are found and detonation ignition and quenching occurs in a cyclic pattern, which eventually leads to a complete detonation re-initiation.

V. Acknowledgement

This study was supported by the National Science Foundation of China (Grant No. 12002207), the Natural Sciences and Engineering Research Council of Canada (Grant No. RGPIN-2023-03309), and Alberta Innovates. The work done at SJTU was also supported by the School of Aeronautics and Astronautics, Shanghai Jiao Tong University. All the computations were carried out on SJTU supercomputing resources (https://hpc.sjtu.edu.cn/).

References

[1] Teodorczyk, A., Lee, J., and Knystautas, R., "Propagation mechanism of quasi-detonations," *Symposium (International) on Combustion*, Vol. 22, Elsevier, 1989, pp. 1723–1731.

[2] Bhattacharjee, R. R., *Experimental investigation of detonation re-initiation mechanisms following a Mach reflection of a quenched detonation*, 2013.

[3] Bhattacharjee, R., Lau-Chapdelaine, S. S. M., Maines, G., Maley, L., and Radulescu, M. I., "Detonation re-initiation mechanism following the Mach reflection of a quenched detonation," *Proceedings of the Combustion Institute*, Vol. 34, No. 2, 2013, pp. 1893–1901.

[4] Floring, G., Peswani, M., and Maxwell, B., "On the role of transverse detonation waves in the re-establishment of attenuated detonations in methane–oxygen," *Combustion and Flame*, Vol. 247, 2023, p. 112497.

[5] Radulescu, M. I., and Maxwell, B. M., "The mechanism of detonation attenuation by a porous medium and its subsequent re-initiation," *Journal of Fluid Mechanics*, Vol. 667, 2011, pp. 96–134.

[6] Chao, J. C., "Critical deflagration waves that lead to the onset of detonation," 2006.

[7] Zhu, Y., Chao, J., and Lee, J., "An experimental investigation of the propagation mechanism of critical deflagration waves that lead to the onset of detonation," *Proceedings of the Combustion Institute*, Vol. 31, No. 2, 2007, pp. 2455–2462.

[8] Ohyagi, S., Obara, T., Hoshi, S., Cai, P., and Yoshihashi, T., "Diffraction and re-initiation of detonations behind a backward-facing step," *Shock Waves*, Vol. 12, 2002, pp. 221–226.

[9] Oran, E. S., and Gamezo, V. N., "Origins of the deflagration-to-detonation transition in gas-phase combustion," *Combustion and flame*, Vol. 148, No. 1-2, 2007, pp. 4–47.

[10] Gamezo, V. N., Ogawa, T., and Oran, E. S., "Numerical simulations of flame propagation and DDT in obstructed channels filled with hydrogen–air mixture," *Proceedings of the Combustion Institute*, Vol. 31, 2007, pp. 2463–2471.

[11] Lu, X., Kaplan, C. R., and Oran, E. S., "Calibrating the chemical-diffusive model using the detonation cell data," *AIAA Scitech 2021 Forum*, 2021, p. 0053.

[12] Gamezo, V. N., Desbordes, D., and Oran, E. S., "Formation and evolution of two-dimensional cellular detonations," *Combustion and Flame*, Vol. 116, No. 1-2, 1999, pp. 154–165.

[13] Khokhlov, A., Austin, J., Pintgen, F., and Shepherd, J., "Numerical Study of the Detonation Wave Structure in Ethylene-oxygen Mixtures," *42nd AIAA Aerospace Sciences Meeting and Exhibit*, American Institute of Aeronautics and Astronautics, Reno, Nevada, 2004.

[14] Sharpe, G. J., and Radulescu, M. I., "Statistical analysis of cellular detonation dynamics from numerical simulations: one-step chemistry," *Combustion Theory and Modelling*, Vol. 15, No. 5, 2011, pp. 691–723.

[15] Lai, S., Xu, C., Davy, M., and Fang, X., "Flame acceleration and transition to detonation in a pre-/main-chamber combustion system," *Physics of Fluids*, Vol. 34, 2022, p. 116105.

[16] Lai, S., Tang, S., Xu, C., Sekularac, N., and Fang, X., "Computational diagnostics for flame acceleration and transition to detonation in a hydrogen/air mixture," *Combustion and Flame*, Vol. 258, 2023, p. 113054.

[17] Gamezo, V. N., Ogawa, T., and Oran, E. S., "Flame acceleration and DDT in channels with obstacles: Effect of obstacle spacing," *Combustion and Flame*, Vol. 155, 2008, pp. 302–315.

[18] Lu, X., Kaplan, C. R., and Oran, E. S., "A chemical-diffusive model for simulating detonative combustion with constrained detonation cell sizes," *Combustion and Flame*, Vol. 230, 2021, p. 111417.

[19] *Parametric Studies of Deflagration-to-Detonation Transition in a Pre-Chamber/Main-Chamber System*, Internal Combustion Engine Division Fall Technical Conference, Vol. ASME 2022 ICE Forward Conference, 2022.

[20] Sharpe, G. J., and Radulescu, M. I., "Statistical analysis of cellular detonation dynamics from numerical simulations: one-step chemistry," *Combustion Theory and Modelling*, Vol. 15, No. 5, 2011, pp. 691–723.

[21] Short, M., and Stewart, D. S., "Cellular detonation stability. Part 1. A normal-mode linear analysis," *Journal of Fluid Mechanics*, Vol. 368, 1998, p. 229–262.

[22] Pintgen, F., and Shepherd, J., "Detonation diffraction in gases," *Combustion and Flame*, Vol. 156, No. 3, 2009, pp. 665–677.

[23] H. Ng, A. H., C. Kiyanda, M. R., Lee, J., Bates, K., and Nikiforakis, N., "Nonlinear dynamics and chaos analysis of one-dimensional pulsating detonations," *Combustion Theory and Modelling*, Vol. 9, No. 1, 2005, pp. 159–170.